Ocean Dynamics
DOI 10.1007/s10236-014-0728-3

A long-term nearshore wave hindcast for Ireland: Atlantic and Irish Sea coasts (1979–2012)

Present wave climate and energy resource assessment

Sarah Gallagher · Roxana Tiron · Frédéric Dias

Received: 22 January 2014 / Accepted: 22 April 2014

Abstract The Northeast Atlantic possesses some of the highest wave energy levels in the world. The recent years have witnessed a renewed interest in harnessing this vast energy potential. Due to the complicated geomorphology of the Irish coast, there can be a significant variation in both the wave and wind climate. Long-term hindcasts with high spatial resolution, properly calibrated against available measurements, provide vital information for future deployments of ocean renewable energy installations. These can aid in the selection of adequate locations for potential deployment and for the planning and design of those marine operations. A 34-year (from 1979 to 2012), high-resolution wave hindcast was performed for Ireland including both the Atlantic and Irish Sea coasts, with a particular focus on the wave energy resource. The wave climate was estimated using the third-generation spectral wave model WAVEWATCH III® version 4.11, the unstructured grid formulation. The wave model was forced with directional wave spectral data and 10-m winds from the European Centre for Medium Range Weather Forecasts (ECMWF) ERA-Interim reanalysis, which is available from 1979 to the present. The model was validated against available observed satellite altimeter and buoy data, particularly in the nearshore, and was found to be excellent. A strong spatial and seasonal variability was found for both significant wave heights, and the wave energy flux, particularly on the north and west coasts. A strong correlation between the North Atlantic Oscillation (NAO) teleconnection pattern and wave heights, wave periods, and peak direction in winter and also, to a lesser extent, in spring was identified.

Keywords Hindcast · Wave climate · Marine renewable energy · Interannual variability · Teleconnection patterns · Ireland

Responsible Editor: Oyvind Breivik

This article is part of the Topical Collection on the *13th International Workshop on Wave Hindcasting and Forecasting in Banff, Alberta, Canada October 27 – November 1, 2013*

S. Gallagher (✉) · R. Tiron · F. Dias
UCD School of Mathematical Sciences,
University College Dublin, Belfield, Dublin 4, Ireland
e-mail: gallags@gmail.com

F. Dias
Centre de Mathématiques et de Leurs Applications,
École Normale Supérieure de Cachan, 94235 Cachan, France

Present Address:
S. Gallagher
Met Éireann, Glasnevin, Dublin 9, Ireland

1 Introduction

Studies aimed at quantifying the variability of the wave climate and energy resource in areas of the Northeast Atlantic, over timescales of a decade or more, have been performed in recent years (for example, Gallagher et al. 2013; Boudière et al. 2013; Charles et al. 2012; Dodet et al. 2010). In the operational wave forecasting community, increased attention is being paid to the nearshore (van der Westhuysen 2012), awakened in part by the potential energy resource but also by an increased awareness of coastal hazards and their possible impacts on coastal communities. Improvements in ocean wave forecasting skill (Janssen 2008) and the availability of high-quality global reanalysis datasets now enable long-term regional and local area wave hindcasts to be performed, downscaling to a high resolution in the nearshore.

Additionally, recent studies have shown that in nearshore locations, wave energy extraction levels could be

Published online: 28 June 2014

commensurate to those found in the offshore (Folley and Whittaker 2009). In addition, the cost of transferring power onshore and the accessibility for maintenance can be improved by the proximity to the coastline.

Most wave climate studies for Ireland have targeted limited nearshore sites (Gallagher et al. 2013; Tiron et al. 2013) and also offshore locations on the Irish west coast (Electricity Supply Board (ESB) 2005; Curé 2011; Rute Bento et al. 2011; Cahill and Lewis 2011). The geomorphology of the Irish west coast is in fact quite heterogeneous and complex. This is likely to introduce significant variability in the wave energy resource for this region (Tiron et al. 2013). In order to investigate this variability, a high-resolution nearshore, 34-year wave hindcast was carried out for Ireland, with a particular focus on the wave energy resource. To complete the wave climate picture, the entire coastline has been modelled, both the Atlantic coast and the eastern seaboard, where the majority of the population is located and where wind-seas dominate.

The wave climate is estimated using the third-generation spectral wave model WAVEWATCH III® version 4.11 (Tolman 2014), the unstructured grid formulation (Roland 2008). The wave model was forced with directional wave spectral data and 10-m winds from the European Centre for Medium Range Weather Forecasts (ECMWF) ERA-Interim reanalysis, which is available from 1979 to the present (Dee et al. 2011; Persson 2011).

The wave hindcast was validated with altimeter data from the Centre de Recherche et d'Exploitation Satellitaire (CERSAT) database (Queffeulou and Croizé-Fillon 2013) and with data from wave buoys located all around the coast of Ireland, in particular with buoys located in nearshore regions. Two such areas on the west coast, which possess steep bathymetry gradients, and complex exposed rocky shorelines, are the southern part of Achill Island on the Co. Mayo coastline and an area centred at Killard point on the Co. Clare coast. For these areas, wave buoy and acoustic Doppler current profiler (ADCP) data for intermediate to shallow depths (50 m or less) was obtained from the WestWave project of the ESB (WestWave 2013). Additionally, nearshore wave buoy data from other areas with more gentle bathymetric gradients (such as Broadhaven Bay, Co. Mayo) is used to validate the wave model. The location and depths of the buoys are described in Fig. 3 and Table 1.

Table 1 Buoy location depth and duration of the time series used in comparison with model data

Buoy	Location	Depth (m)	Period (mm/yyyy)
M3	SW of Mizen Head	155	01/2003–12/2012
M1	W of Aran Isl.	140	03/2001–12/2007
BH4	W of Belmullet	100	05/2012–12/2012
M2	E of Lambay Isl.	95	05/2003–12/2012
M4	Donegal Bay	72	04/2003–11/2012
M5	SE Coast	70	10/2004–12/2012
BH3	W of Belmullet	56	12/2009–01/2012
K1	Killard Point	51	11/2011–01/2012
AC1	Achill Isl.	43	11/2011–08/2012
BH1	Broadhaven Bay	38	01/2009–10/2009
K2	Killard Point	36	08/2012–12/2012
SB2	E of Aran Isl.	28	01/2010–06/2010
G1	Galway Bay	22	05/2008–01/2012
AC2	Achill Isl.	21	11/2011–01/2012
SB1	Mace Head	18	04/2009–09/2009
BH2	Broadhaven Bay	11	06/2009–07/2009

Buoys listed in order of depth

2 Construction of the wave hindcast model

2.1 The digital elevation model

The quality of the bathymetric data used to build the computational grid greatly influences the accuracy of wave models in the nearshore. Historical seabed surveys have substantial uncertainties which only recently came under the scrutiny of the hydrographic community (Calder 2006). These uncertainties are related to the survey methodology, interpolation of the scattered survey data and any changes in the seabed topography that may have occurred over time, after the bathymetric survey was carried out.

Modern and highly accurate survey techniques such as light detection and ranging (LIDAR) or multi-beam echo-sounder (MBES) are currently used to map nearshore areas in campaigns such as the Integrated Mapping For the Sustainable Development of Ireland's Marine Resource (INFOMAR 2006), which is a successor to the Irish National Seabed Survey (INSS), as described by Dorschel et al. (2011). However, it may take several years for mapping of the Irish seabed to be completed.

In the interim, digital elevation models (DEMs) have to combine sets of data with varying degrees of accuracy and resolution. The level of accuracy of a DEM has an impact on coastal hydrodynamical models (for example, wave or circulation models) and, if not accounted for, could lead to erroneous interpretations of the results (Calder 2006). Recent efforts have been made to construct DEMs with uncertainty estimates (Poti et al. 2012).

The final DEM for Ireland (see Fig. 3) was obtained by merging three bathymetric sources (shown in Fig. 1):

1. Vector data obtained from OceanWise Ltd., derived from the United Kingdom Hydrological Office (UKHO) admiralty charts. The quality of this data is

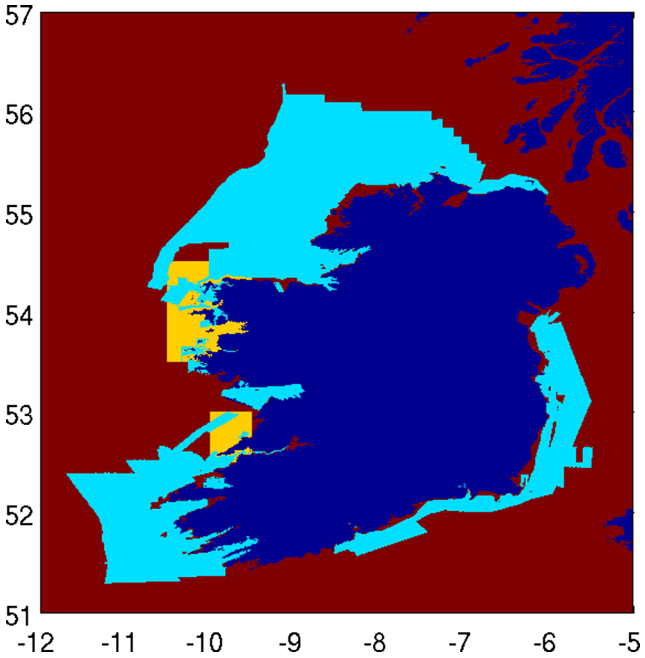

Fig. 1 Bathymetric datasets used in building the DEM for Irish coastal waters: INFOMAR (*light-blue*), UKHO (*yellow*) and EMODnet (*red*) bathymetry. The land is depicted with *blue*

not uniform, and some of the surveys predate modern techniques;

2. The European Marine Observation and Data Network (EMODnet 2013) bathymetric dataset. This dataset has a resolution of approximately 500 m and blends bathymetric datasets from many sources in Europe. It is constantly updated with new surveys, so the quality will continue to improve;
3. High-resolution MBES and LIDAR INFOMAR survey data. Approximately 50 gridded datasets, with resolutions from 2 to 80 m were used.

The mismatch between the coarser datasets (EMODnet and UKHO) and the high-resolution/high-quality INFOMAR dataset was evaluated on areas of overlap. Differences of more than 20 m were observed in some nearshore locations (Tiron et al. 2013). The EMODnet dataset was found to be less accurate than the UKHO data in some nearshore areas on the west coast. Based on this observation, we have ranked the datasets in the order of accuracy (INFOMAR, UKHO and EMODnet).

To avoid artificial ridges at the boundaries between these datasets (which are likely to induce spurious refraction effects and numerical instabilities in the hydrodynamical model), a blending and smoothing procedure was then applied. The datasets were first gridded on a common grid with a resolution of 50 m. Smoothing was applied if the original data was at a finer resolution than the target grid. The overlap areas were excluded from the coarse resolution datasets, based on the ranking mentioned above. Weights of 10, 5 and 1 were assigned to each of the datasets, respectively, and a smoothing kernel with a variable radius based on depth was applied. The radius of smoothing varies between 100 m ($r_{\min}$) for depths smaller than 22 m (h_0) to 2.5 km ($r_{\max}$) in the offshore area:

$$r_{\min} + \frac{r_{\max} - r_{\min}}{2} \left[1 + \tanh\left(\lambda(h - h_0)\right)\right], \quad (1)$$

where $\lambda = 0.2$.

2.2 Wave model description

The wave model grid is an unstructured triangular grid with a resolution varying from 250 m in the nearshore to 10 km in the offshore. The coast and island boundaries were derived from the Global Self-consistent Hierarchical High-resolution Shoreline (GSHHS) database (Wessel and Smith 1996), the finest resolution version, smoothed and sampled at approximately 250 m. Geo-referenced satellite imagery (LANDSAT 2013) was used to correct the coastline and islands. It is worth noting that there are some areas on the west coast of Ireland where a significant mismatch between GSHHS and the shoreline can be seen (see, for example, Tiron et al. 2013).

The resulting grid has approximately 15,000 nodes with a maximum resolution of 250 m in the nearshore (resolved to a depth of 5 m from the shoreline). The outer boundary of the grid was chosen to align with ERA-Interim wave model grid points (see Fig. 2). The boundary feeding was set at grid nodes on segments of the open boundary (in between, and at, the ERA-Interim grid points) where depths were larger than 90 m. The spectral domain was discretized in 24 directions and 30 frequencies logarithmically spaced with an increment of 1.1 from 0.0345 Hz, which coincides with the resolution of the ERA-Interim wave spectra used to force the model. The temporal resolution of the boundary feeding, and of the 10-m ERA-Interim wind forcing fields, is 6 h (the four standard synoptic times). The winds were kept constant on six-hourly intervals centred at the synoptic times. The spatial resolution of the ERA-Interim winds is approximately 79 km (Dee et al. 2011). The default WAVEWATCH III® physical parameterisation switches were employed, with the exception of the *ST4* input and dissipation source term package (see Tolman (2014) for all switch details). This allows for improved parametrisation of source terms and dissipation as formulated by Ardhuin et al. (2010). The model parameterisation formulation TEST451, as described by Ardhuin et al. (2010), was selected. This parameterisation produced the smallest verification errors when tested in the study area. TEST451 also generally provides improved results at the global scale using ECMWF winds (Tolman 2014; Rascle and Ardhuin 2013).

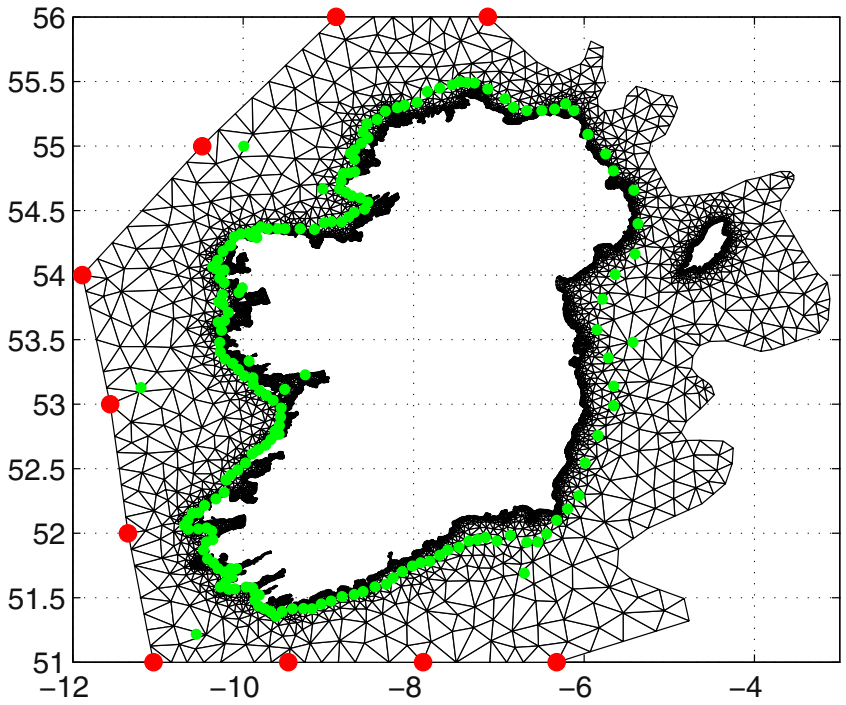

Fig. 2 The wave model grid. *Red* ERA-Interim wave model points used for boundary feeding. *Green* points where three-hourly directional spectra outputs were generated

Hourly field outputs were produced for standard mean wave parameters (significant wave height, standard wave periods, directions), the wave energy flux, spectral partitions parameters and wave-ocean layer parameters. Additionally, the directional spectra was saved every 3 h at the buoy locations and at points on the 60-m depth contour, as can be seen in Fig. 2.

3 Validation of the wave model

3.1 Wave buoys

The wave model was validated with data from 17 different wave buoys located around the Irish coastline as shown in Fig. 3. These buoys vary in depth from 155 to 11 m, as described in Table 1. It should be noted that the Irish Marine Weather Buoy Network, maintained by Met Éireann and the Marine Institute (MI 2013), has only been in operation since 2001, when the first buoy was deployed. Additionally, buoy data in the nearshore has only become available in recent years, predominantly on the west coast, targeting potential wave energy testing and deployment sites, as it can also be seen Table 1.

The comparison between model and observations using statistical quality indexes for significant wave height (Hs), period and direction is summarised in Table 2. Taylor diagrams (Taylor 2001) for Hs, period and direction are shown in Fig. 4. A separation of the results by depth is shown for clarity, with offshore buoys (depths $>$ 60 m) shown with black symbols and nearshore buoys (depths $<$ 60 m) shown with red symbols. Generally, the model appears to perform well when compared to the measured values. The correlation coefficients for significant wave heights are over 0.94 with the exception of 0.89 for the SB2 buoy (located in Galway Bay, in the shadow of the Aran Islands).

A significant bias in Hs can be seen for SB1 (over 40 %). This buoy is located in an area where only EMODnet bathymetry was available, with shallow depths of under 20 m. Interestingly, the correlation coefficient is very good for this location. The observed discrepancy raises questions regarding the accuracy of the bathymetry dataset in this region and in particular for these depth ranges.

Generally, directional biases are under 10° with the exception of the M2 buoy in the Irish Sea and the SB2 buoy, where the direction might be affected by the shadowing effect of the Aran Islands.

The Taylor diagrams in Fig. 4 offer a condensed picture of the overall quality of the model, allowing the assessment of spatial variability in the model's performance. For significant wave height, the model performance is quite homogeneous. In contrast, for the zero-crossing period, a lower performance of the model is quite evident for some sheltered/wind-sea-dominated locations (G1, SB1, SB2 in the Galway Bay area and M2 in the Irish Sea), where mean periods of 4.1 to 4.7 s can be seen (Table 2). At the same time, for offshore buoys on the west coast, the correlation coefficients for period are exceeding 0.8. Correlations for direction are overall larger than 0.65 (better performance

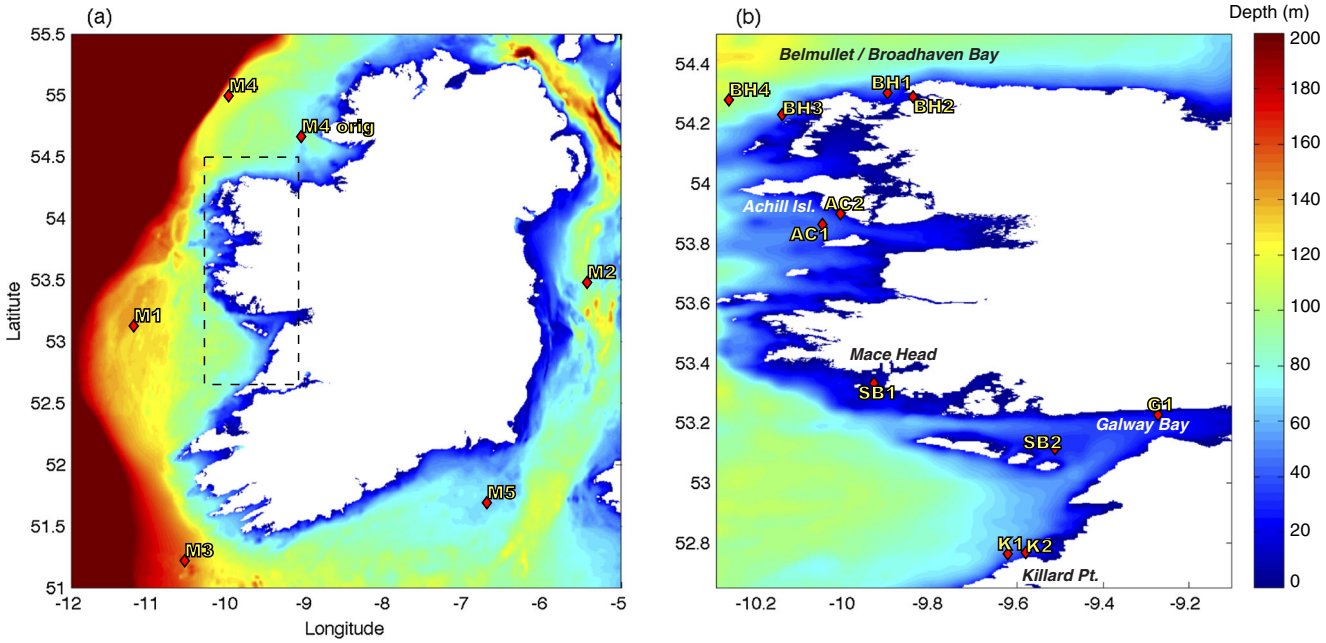

Fig. 3 DEM for Irish coastal waters (resulting from the merging of the bathymetric datasets shown in Fig. 1) and the locations of the buoys used for validation of the wave model hindcast. **a** Locations of the M-buoys from the Irish Marine Weather Buoy Network with the *inset* (*dashed box*) representing the area shown in panel (**b**). **b** Locations of the nearshore buoys. The buoy availability ranges from time periods of a few weeks to almost 10 years, as can be seen in Table 1. Depth is shown positive down

Table 2 Comparison between the model and buoy for significant wave height (Hs), period and direction: the mean of the buoy (X), the bias, the root-mean-square error (RMSE), the correlation coefficient (R) and the scatter index (SI) are shown

	Hs					Period					Direction				
Buoy	X (m)	Bias (cm)	RMSE (cm)	R	SI (%)	X (s)	Bias (s)	RMSE (s)	R	SI (%)	X (deg)	Bias (deg)	RMSE (deg)	R	SI (%)
M3	2.86	−4	45	0.95	16	6.9	0.3	0.8	0.87	11	275	5	13	0.95	15
M1	2.94	−15	46	0.96	16	7.3	0.3	0.9	0.86	12	–	–	–	–	–
BH4	2.87	5	38	0.96	13	6.7	0.2	0.6	0.92	8	292[a]	9	20	0.7	29
M2	1.19	15	31	0.94	25	4.5	0.9	1.2	0.65	26	189	−15	24	0.77	14
M4	3.11	−1	39	0.97	13	7	0.2	0.7	0.98	19	275	2	13	0.94	15
M4 (old)	2.34	−24	55	0.94	23	6.7	0.3	0.9	0.84	13	–	–	–	–	–
M5	1.81	−3	38	0.94	21	5.5	0.1	0.8	0.82	15	231	−6	18	0.84	14
BH3	2.77	11	40	0.97	15	7	0.2	0.7	0.89	10	296[a]	7	16	0.69	25
K1	4.57	31	53	0.97	12	8	0.0	0.7	0.88	7	291[a]	4	9	0.74	13
AC1	2.32	−14	34	0.98	15	6.3	−0.1	0.7	0.91	11	270[a]	5	13	0.68	14
BH1	1.90	2	31	0.97	16	6.2	0.1	0.9	0.86	14	317	4	11	0.83	25
K2	2.44	20	40	0.96	16	6.7	0.0	0.7	0.90	11	292[a]	−0.5	9	0.75	13
SB2	0.62	−5	17	0.89	27	4.3	−0.4	1.9	0.61	43	259	12	29	0.65	29
G1	0.75	7	18	0.94	25	4.1	−0.3	1.5	0.60	6	–	–	–	–	–
AC2	3.79	−6	43	0.95	11	12.3[a]	−0.5	1.5	0.76	12	260[a]	6	12	0.45	12
SB1	0.85	−36	44	0.95	52	4.7	−0.4	1.1	0.71	23	230	6	12	0.70	9
BH2	0.36	1	8	0.97	15	–	–	–	–	–	–	–	–	–	–

Where possible, the zero-crossing period and mean direction were used. In some locations, only the peak period or peak direction was available. All directional error statistics were calculated using the circular statistics toolbox from Berens (2009)

[a]Comparisons were between the buoy and model peak period or peak direction, respectively

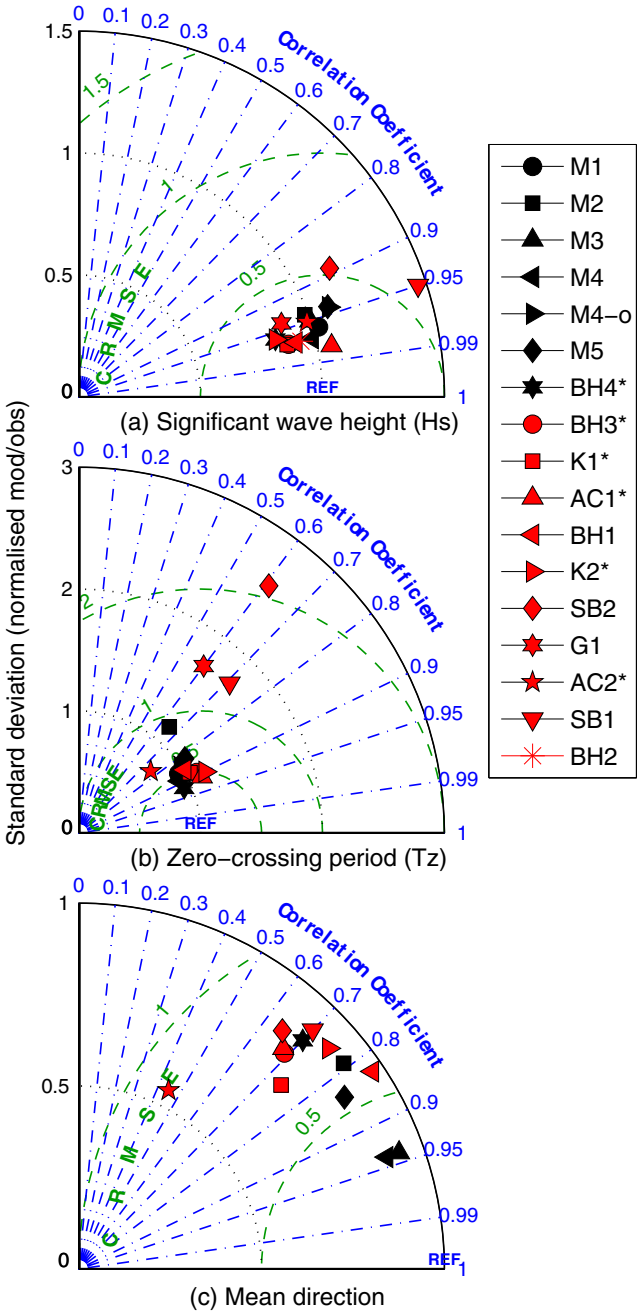

Fig. 4 *Top panel* (**a**) Hs, *middle panel* (**b**) zero-crossing period, and *bottom panel* (**c**) mean direction. Taylor diagrams (showing a statistical comparison in terms of correlation, centred root-mean-square error (*CRMSE*) and the ratio of standard deviation) between the buoy observations and the model. Further statistical comparisons can be seen in Table 2. Additional separation of the results by depth can be seen with offshore buoys with depths > 60 m shown with *black symbols* and nearshore buoys with depths < 60 m shown in *red*. (The *asterisk* denotes where comparisons were between the buoy and peak direction instead of mean direction, with the exception of AC2 buoy, where the comparison was between the model and both peak period and peak direction from the buoy, respectively)

for the offshore locations being evident), with the exception of AC2. Nonetheless, at this nearshore location (water depth 21 m), refraction affects direction strongly (the standard deviation of the measured direction is 11.7°), and the bias between model and measurements is only 6°.

3.2 Altimeter data

Satellite-derived wave data can provide an additional method to verify the wave models' performance. Altimeter wave data is reliable only in the open ocean, up to tens of kilometres from the coast (data in the coastal zone is often discarded). Recently, work has been carried out to improve satellite-derived measurements in the nearshore coastal zone, such as the COASTALT Project (COASTALT 2014). Currently, however, only altimeter data from the open ocean can provide reliable wave measurements. Altimeter data can provide a way to further validate the hindcast in areas with little or no buoy records available, as is the case on the eastern seaboard of Ireland, where presently there is only one buoy (M2). This data provides a good spatial description of the wave climate, although the temporal resolution is low due to the long repeat cycle orbits of the various satellites (as detailed in Table 3). The CERSAT altimeter database was used to compare with model results (CERSAT 2013). The CERSAT database data was obtained from the CERSAT, at Ifremer, Plouzané, France. They were produced in the framework of the GlobWave project (GlobWave 2013), funded by the European Space Agency (ESA). These altimeter-derived measurements have been calibrated and corrected in a previous work by Queffeulou and Croizé-Fillon (2013). This data provides an almost continuous 21-year record with which the wave model was compared. The different altimeter missions include ERS-1&2, TOPEX-Poseidon, GEOSAT Follow-ON (GFO), Jason-1, Jason-2, ENVISAT and Cryosat-2. The tracks over the wave model area for all of 2006 can be seen in Fig. 5.

Altimeters typically yield one second mean values, with a 6–7-km resolution (GlobWave 2013). The wave model hindcast has a varying resolution of approximately 10 km (offshore) to 250 m (in the very nearshore) and a temporal resolution of 1 h. In order to compare Hs from the two datasets, the nearest model Hs was interpolated onto the position of the altimeter tracks. The results of this spatiotemporal comparison between the satellite data and the model data (interpolated to collocate along the satellite tracks) are summarised in the statistical quality indexes shown in Table 4. These global statistics show a low model bias of 7 cm in Hs. This corresponds to a relative bias (normalised by the observed mean) of only 3 % and a very good agreement overall between the model and satellite data.

Table 3 Summary of the altimeter data extracted from the CERSAT database that was used to validate the wave model hindcast

Details of the calibrations applied to the dataset can be found in Queffeulou and Croizé-Fillon (2013)

Satellite	Repeat cycle (days)	Period
ESA ERS-1	35	August 1991–June 1996
ESA ERS-2	35	May 1995–July 2011
ESA Envisat	35 (pre October 2010)	May 2002–April 2012
	30 (post November 2010)	
CNES/NASA TOPEX/Posidon	10	September 1992–October 2005
CNES/NASA Jason-1	10	January 2002–present
CNES/NASA Jason-2	10	July 2008 - present
US Navy/NOAA GFO	17	January 2000–September 2008
ESA/NOAA CryoSAT-2	30 (pseudo cycle)	January 2012–present

A breakdown by satellite can be seen in Fig. 6 panel a, which shows a Taylor diagram of the model versus measurements. The similarity of the statistics confirms consistency in the quality of the satellite measurements of wave heights over the area of interest. As can be seen from the quantile-quantile Q-Q plot in Fig. 6 panel b, the model begins to slightly underestimate Hs values above 8 m. This is consistent with that of Tolman (2014), which mentions a known low bias for WAVEWATCH III® using the TEST451 parameterisation and ECMWF winds. This is also evidenced by the heavier positive tail of the histogram of differences between observed (altimeter) and model displayed in Fig. 6 panel c.

A regional examination of the model performance was undertaken, to take into account the very different wave climate regimes that exist around Ireland between the Atlantic Ocean (swell dominated, mean Hs of 2.69 m) and the Irish Sea (wind-sea dominated, mean Hs of 1.29 m). The different wave climate regimes are discussed further in Section 4 and can be seen in Fig. 10. The Irish Sea area was defined as the part of the wave model domain east of −6.4° W in longitude, between the 51.75° N and 55.25° N parallels. The Atlantic and Celtic Sea regions were defined, for the purposes of the comparison, as all of the model domains except for the region that is both east of −6.4° W and north of 51.75° N (i.e. the Irish Sea and the Firth of Clyde).

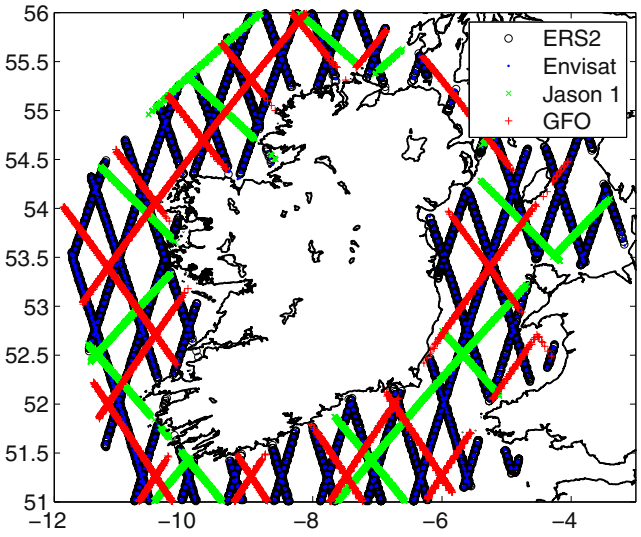

Fig. 5 Satellite altimeter tracks over the wave model area during 2006

Looking at Table 4, the relative bias for the Atlantic and Celtic Sea regions covered by the wave model is less than 2 %. The statistical comparison for the Irish Sea (Table 4) shows a much larger relative bias of over 9 % (12 cm). The lower performance of the model in this region with respect to the Atlantic coast can also be seen in Fig. 7 panel a. This is consistent with the results of the M2 buoy comparison with the model, where the bias of 15 cm, or a relative bias of over 12 % as can be seen in Table 2. A lower correlation and a much larger scatter index and spread in the data can also be found in the Irish Sea area as can be seen in Fig. 7, where scatter plots of the Irish Sea and Atlantic model results versus the altimeter data are shown for Hs. The fact that the wind forcing for the hindcast has a relatively coarse resolution of 79 km, and might therefore be too coarse to capture some localised mesoscale wind effects, especially due to orography, could explain the small drop in model

Table 4 Global comparison from 1991 to 2012 (21 years) between the model and satellite altimeter data from the CERSAT database for significant wave height (Hs): the mean of the satellite (X), the bias, the root-mean-square error (RMSE), the correlation coefficient (R) and the scatter index (SI) are shown

Hs	Number of points	X (m)	Bias (cm)	RMSE (cm)	R	SI (%)
All areas	523,471	2.29	7	39	0.97	17
Atlantic and Celtic Sea	376,099	2.69	5	39	0.97	15
Irish Sea	144,453	1.29	12	38	0.91	29

See Table 3 for details of the different altimeter campaigns

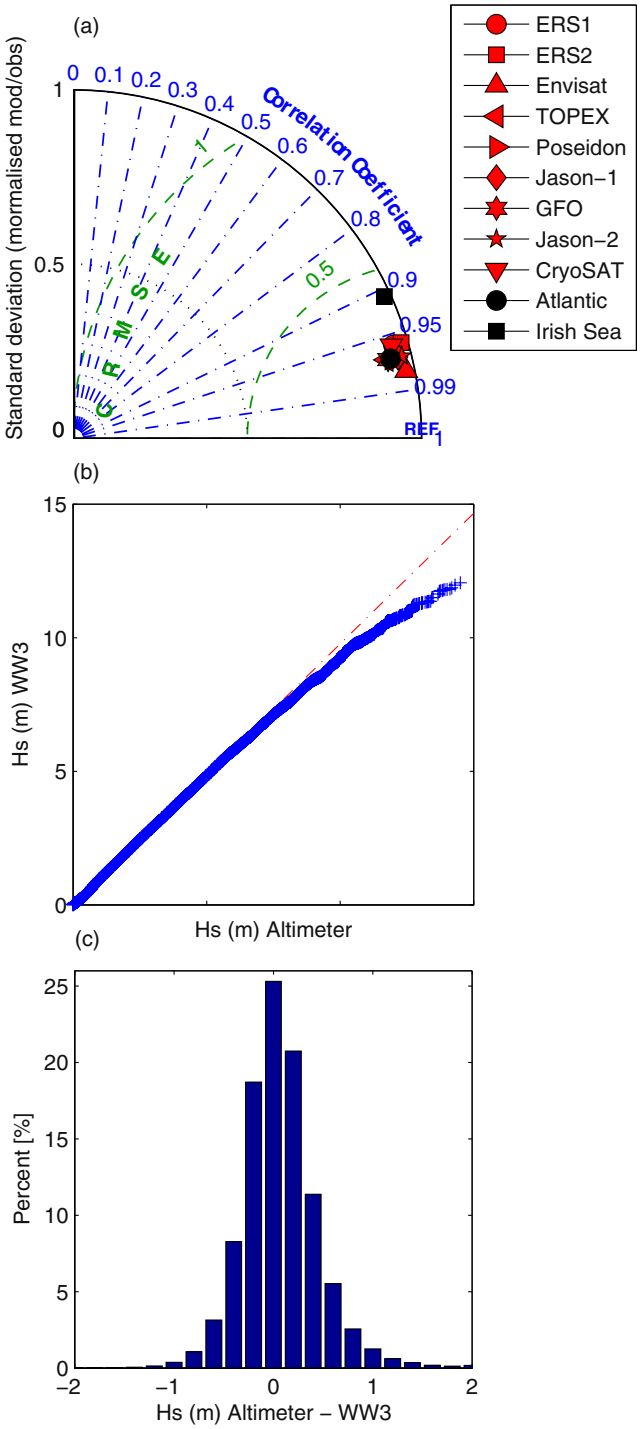

Fig. 6 Global comparison between altimeter and model, for the period of 1991–2012 (at all collocated track points). *Top panel* (**a**) Taylor plot of the wave model versus the CERSAT satellite altimeter database (global comparison). *Middle panel* (**b**) *Q*-*Q* plot of the global satellite altimeter data versus Hs of the wave model (WW3). *Bottom panel* (**c**) A histogram of the difference between altimeter and model for Hs at the collocated track points (0.2-m bins)

performance in the Irish Sea region. These forcing wind fields would need to be of sufficient resolution to reflect the

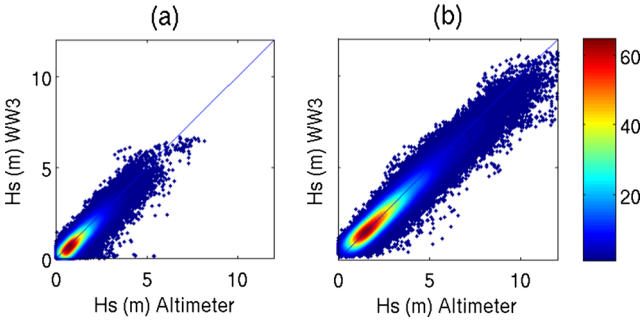

Fig. 7 Scatter diagrams of altimeter versus model Hs (m). Model data interpolated onto satellite tracks. *Colours* indicate density of points. **a** Irish Sea area. **b** Atlantic and Celtic Sea areas

small-scale features associated with the coastline of the Irish Sea basin and the sheltering effects of bays and islands. A downscaling of the wind forcing, to capture better this wind-sea-dominated area has been shown to improve the model performance. For details, see Dias et al. (2013), where a shorter-term (13 years) hindcast for Ireland is presented, forced with high-resolution winds. In fact, to examine further some of the statistical quality indexes spatially, we have compared the ERA-Interim 10-m wind forcing fields to altimeter-measured wind speeds over the model area; see Fig. 8. ERA-Interim 10-m winds and altimeter wind

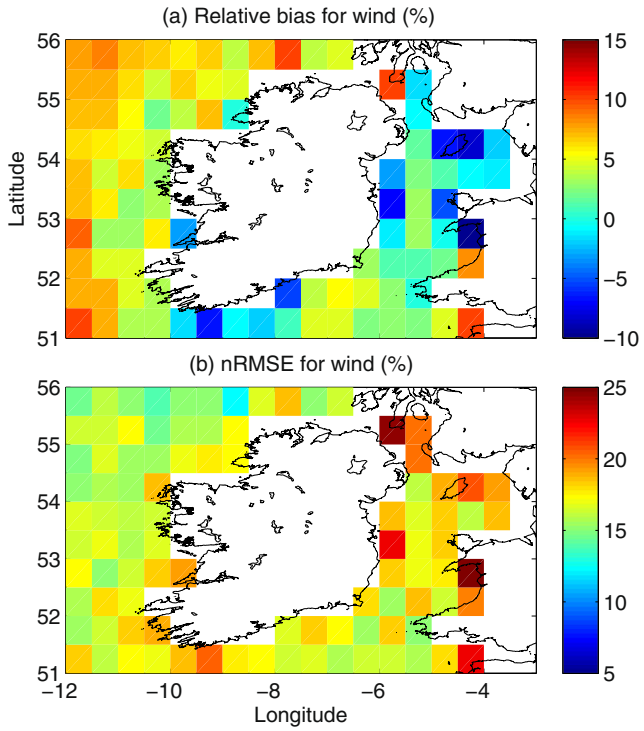

Fig. 8 Spatial quality index maps for wind of the collocated CERSAT satellite altimeter data (observed) versus the wave model driving 10-m winds, from the ECMWF ERA-Interim reanalysis, for the period of 1991–2012. *Top panel* (**a**) Relative bias (%). *Bottom panel* (**b**) Normalised root-mean-square error (%)

speeds (over the 21-year period of altimeter data) were collocated along the satellite tracks (using 6-h windows centred on the synoptic times) and were then interpolated to a regular grid by averaging along the tracks in a 0.5° latitude by 0.5° longitude grid. An overall low bias of approximately 5 % can be seen (panel a of Fig. 8). Note the increased variability in the bias in the Irish Sea region and also a higher nRMSE (panel b of Fig. 8). A high bias is present over islands and close to the shore, in areas where sheltering effects are not resolved by the resolution of the model. It is evident that the wind forcing does not have sufficient resolution to resolve such a small sea basin.

Spatial quality index maps were also used to examine further the wave model hindcast performance of Hs. Altimeter and wave model Hs results, already collocated (spatially and temporally) along the satellite tracks, were interpolated to a regular grid by averaging along the tracks in a 0.2° latitude by 0.2° longitude grid. Using this collocated data, the overall mean Hs, the relative bias and normalised root-mean-square error (nRMSE) can be seen in a spatial context in Fig. 9. (Similar methods have been employed as part of the GlobWave project by Appendini and Camacho (2012), collocating data to examine spatial quality index maps and by Liberti et al. (2013), although no temporal or spatial interpolation was carried out as the nearest grid cell was used for the statistical comparison.)

Comparing the overall altimeter mean Hs in Fig. 9 panel a, to the annual mean shown in Fig. 11 from the analysis of the wave model hindcast Hs, the overall pattern is similar. The relative bias and nRMSE show the lower performance of the hindcast in the Irish Sea. As discussed previously, this could be due to the relatively low-resolution forcing wind fields, which prevent the adequate modelling of wind-sea growth in the wind-dominated Irish Sea. Looking at the western seaboard, the relative bias is generally less than ±3 %. This is consistent with Table 2 where the biases for buoys on the west coast vary between negative and positive, although the variability and magnitude of the relative bias is larger when comparing the buoy and model data. For example, the BH3 buoy has a low relative bias of 4 %, while the M1 buoy has a high relative bias of −5 %. Looking at Fig. 9, the largest relative biases are on the south coast in the Celtic Sea region which show a negative relative bias (a high bias mostly between −1 and −4 %) overall. The M3 buoy located in this region (see Fig. 3 for location and Table 2 for quality index statistics) was found to have a negative relative or high bias of −1.4 %, consistent with the findings of the re-gridded collocated model and altimeter data in Fig. 9.

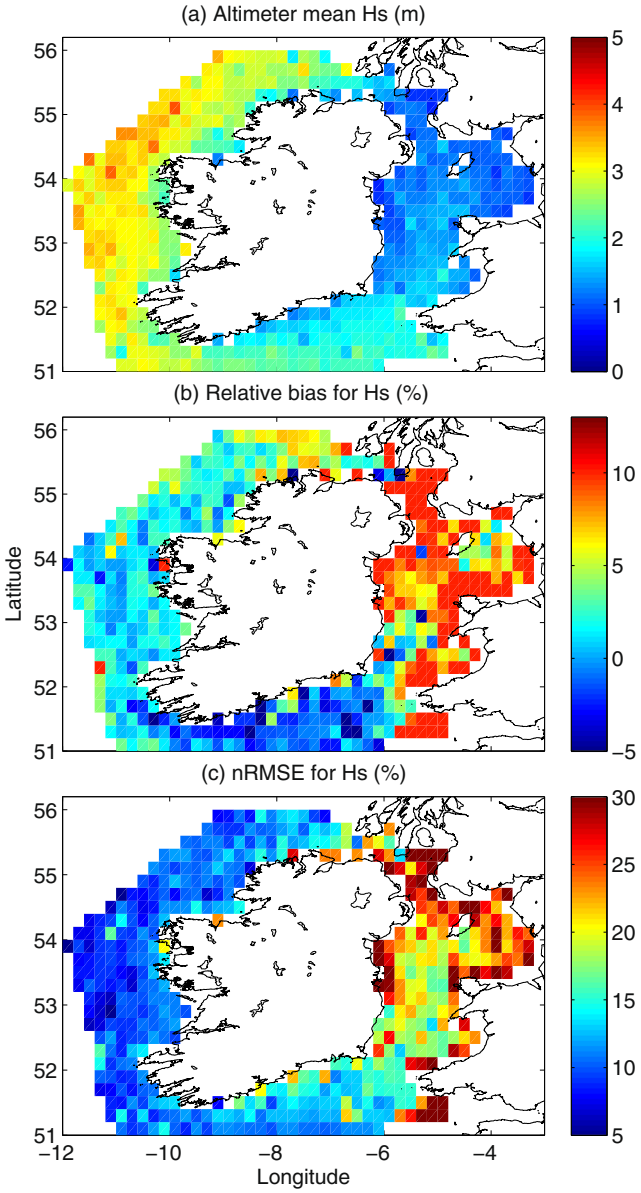

Fig. 9 Spatial quality index maps for Hs (m) of the collocated CERSAT satellite altimeter data (observed) and the wave model hindcast (WW3) 1991–2012. *Top panel* (**a**) Mean Hs (m). *Middle panel* (**b**) Relative bias (%). *Bottom panel* (**c**) Normalised root-mean-square error (%)

4 Characterisation of the present wave climate of Ireland

In this section, the wave climate of Ireland during the period of 1979–2012 is characterised, based on the hindcast introduced in the preceding sections of this article. The goal is to compose an overall picture of wave climate variability around the Irish coast and in particular to contrast the Atlantic west and southern coasts to the milder wind-dominated Irish Sea coast. As such, the details gained in describing the wave climate in the nearshore are perhaps

not immediately apparent in this analysis. As shown in Section 3.1, the hindcast results compare favourably with measurements from buoys in water depths as low as 20 m and thus offer a detailed picture of the nearshore wave climate of Ireland. Further analysis focusing on regions close to the coastline will be performed in the near future. A look at the overall average of the wind-sea fraction of the wave energy spectra (presented in Fig. 10) reveals three areas with distinct wave climate regimes. The local winds are responsible for more than 60 % of the wave energy in the Irish Sea. On the southern coast, the swell and wind-sea components are equally represented, whereas the west coast is swell dominated, with the exception of areas where the Atlantic swells are attenuated by islands or in bays and inlets. It is interesting to note that the hindcast quality appears to degrade with higher wind-sea fraction values (see, for instance, Fig. 9 where spatial quality index maps for the model performance by comparison to satellite data are shown). This fact offers supplementary evidence for the insufficient spatial resolution of the forcing wind fields employed in the current hindcast as discussed previously in Section 3.2.

4.1 Seasonal means and interannual variability

In the following section, we focus on the spatial, seasonal and interannual variability of mean wave parameters of interest. The annual and seasonal means for significant wave height are shown in Fig. 11, left panels. The right panels show the normalised standard deviation of the annual means (%) which quantifies the variability from year to year.

The overall means display a pronounced spatial variation around the coast: from 3 m off the west coast to less than 1 m in the Irish Sea. The southwest to the northwest exhibit the largest levels of Hs, and, in fact, these patterns are preserved for all seasons. The largest values of Hs can be seen in winter off the west coast (close to 5 m). In contrast, mean

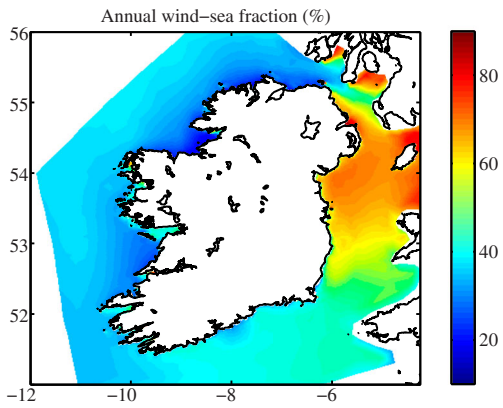

Fig. 10 Average of the wind-sea fraction of the wave energy spectra for the period of 1979–2012 (%)

Hs values do not exceed 2 m on the Irish Sea coast in any season. The spring and autumn means are very similar (and commensurate with the overall annual mean). This is in fact the case for all mean wave parameters.

The Irish wave climate presents significant interannual variability in terms of Hs: overall less than 15 % for the annual means but up to 25 % in winter and spring. On the Atlantic coast, the interannual variability is more pronounced in the nearshore.

Figure 12 displays the annual and seasonal means for the wave power per metre of wave crest (upper panels) and the normalised standard deviation of the yearly means, percentage (lower panels). The wave power per metre of wave crest is defined as follows:

$$J = \rho_{\mathrm{w}} g E \overline{c}_{\mathrm{g}}\,, \tag{2}$$

with ρ_{w} being the density of water, g the gravity acceleration, E the first moment of the frequency-direction spectrum and c_{g} the averaged group velocity taken over the frequency-direction spectrum (Tolman 2014). The focus is on the west coast, since the power levels typically seen on the south and east coasts are quite reduced, and thus these areas are not targeted as potential sites for wave energy converter farms.

In winter, the Atlantic coast is exposed to highly energetic sea states (over 100 kW/m), which do not dissipate significantly until very close to the shoreline. It is important to note in this context that wave energy converters (WECs) are typically designed to extract energy up to a certain level above which they are not safe to operate. A more accurate measure of the wave energy resource would have to take into account these limitations (Folley and Whittaker 2009). It is thus expected that the exploitable energy levels in winter are substantially smaller. The decrease in energy levels from winter to summer is quite dramatic, even though on the west coast, energy levels of up to 20 kW/m are maintained in summer months. For the wave power level, the variability from year to year is markedly larger than for Hs, as evident in Fig. 12—around 20 % for the annual mean and over 50 % in spring.

The Irish wave climate exhibits little seasonal variability in terms of direction. In Fig. 13, the overall average of the mean and peak wave direction for the period of 1979–2012 is displayed. (The circular mean was evaluated for all directional quantities.) The predominant incoming wave direction on the Atlantic coast is west to southwest (with only a slight 10–20° southerly shift from the west direction). In the southwest of Ireland and in a small area from the Dingle peninsula up to the Loop head, the predominant direction is from the west.

On the Irish Sea coast, waves come predominantly from a southerly direction. The same mean direction can be seen on the southern coast of Ireland. The average peak direction is very similar to the mean direction. However, a small

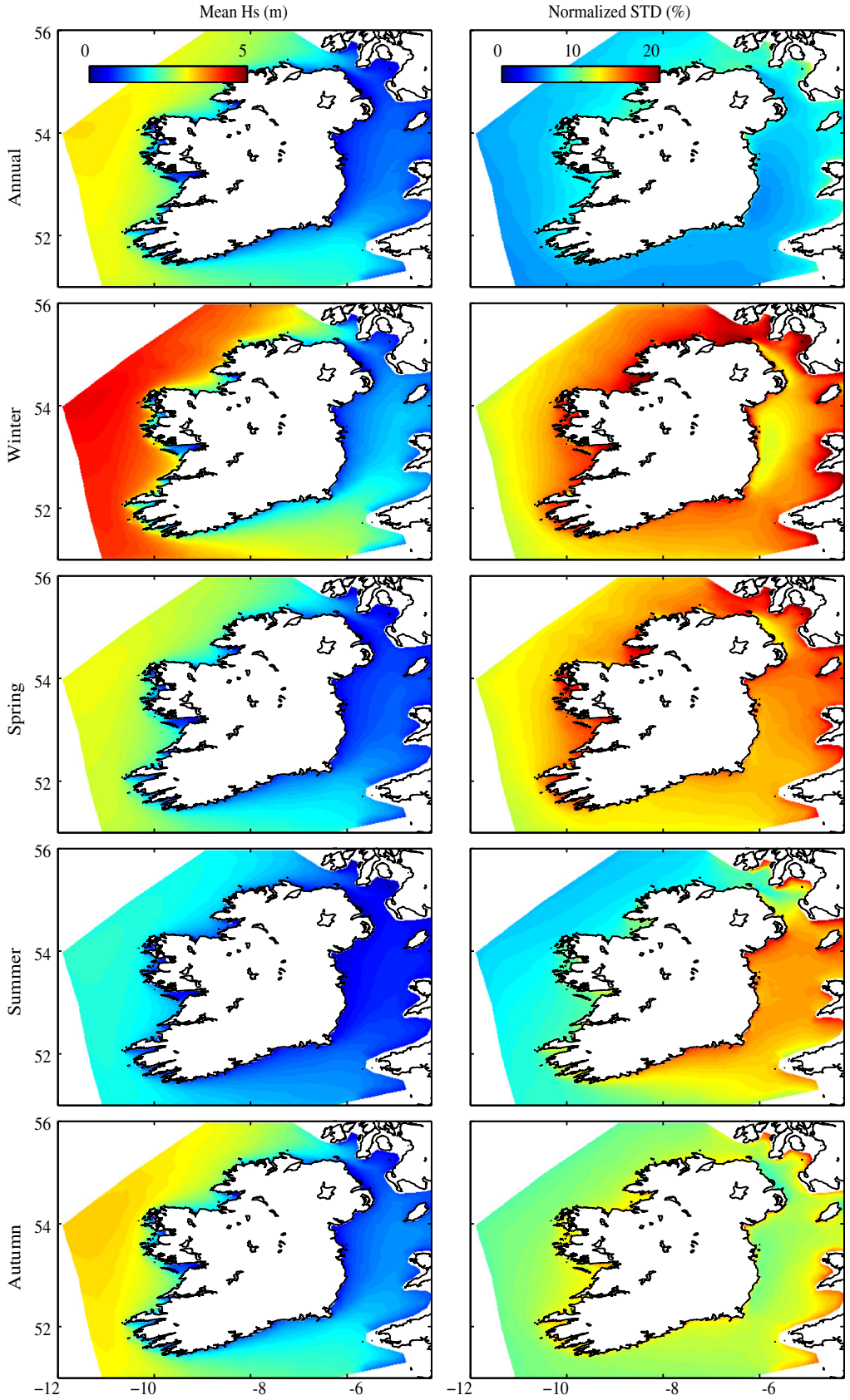

Fig. 11 Significant wave height (m) for the period of 1979 to 2012. *Left panels* annual and seasonal means. *Right panels* normalised standard deviation of the yearly means (%) which is a measure of the interannual variability

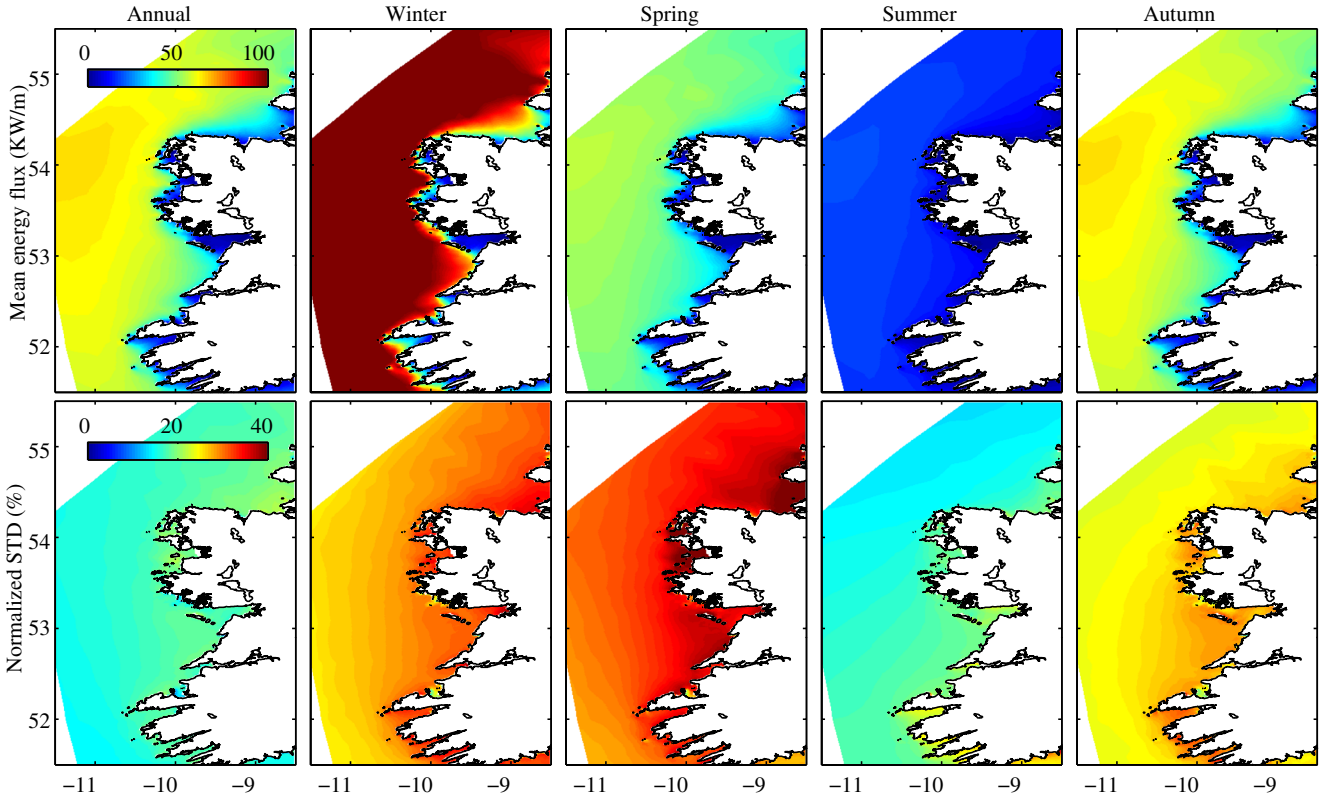

Fig. 12 Wave power per unit crest (kW/m) for the period of 1979 to 2012. *Upper panels* annual and seasonal means. *Lower panels* normalised standard deviation of the means (%) which is a measure of the interannual variability of the wave energy resource

northerly shift in peak direction with respect to the mean direction can be seen off the northwest coast.

4.2 Correlation with atmospheric teleconnection patterns

As the generating mechanism of ocean surface waves consists in surface winds, global atmospheric circulation patterns and wave climate characteristics are intimately connected.

The strong interannual variability of the Irish wave climate (evidenced in Figs. 11 and 12) can be in fact linked to larger-scale atmospheric circulation patterns. Several studies have identified strong correlations between the Atlantic wave climate averages and various teleconnection indices, in particular, the North Atlantic Oscillation (NAO) and the East Atlantic (EA) teleconnection pattern (Barnston and Livezey 1987) at the whole Atlantic basin scale (Wang and Swail 2001, 2002) and also for the Northeast Atlantic region

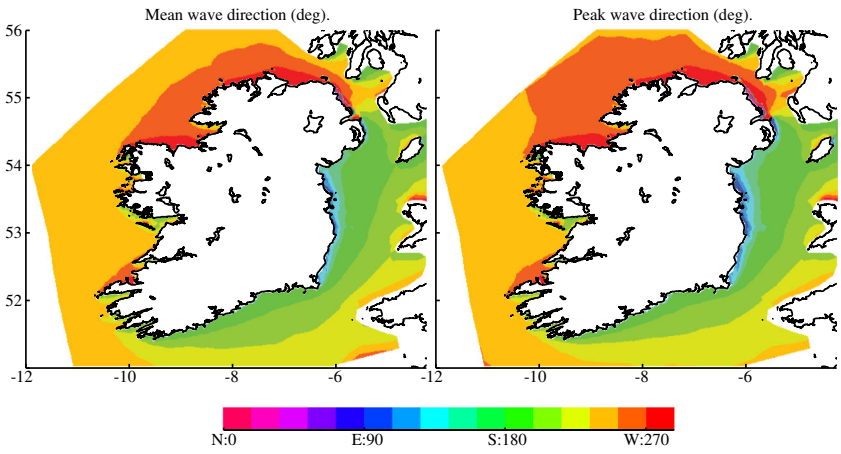

Fig. 13 Directionality of the Irish wave climate for the period of 1979 to 2012. *Left panel* annual average mean wave direction (deg). *Right panel* annual average peak wave direction (deg). Directions are given in the meteorological convention: 0° corresponds to waves coming from the north, and 90° corresponds to waves coming from the east

(see, for example, recent studies by Charles et al. 2012; Le Cozannet et al. 2010; Bertin et al. 2013; Dodet et al. 2010).

Local winds play an important role in the Irish wave climate, in particular in the Irish Sea (as Fig. 10 shows). At the same time, the swells generated in the North Atlantic basin, which propagate long distances before reaching Ireland, are prevalent on the west coast. As a consequence, the wave climate around the Irish coast is quite heterogeneous. With this in mind, we evaluate the correlation between the predominant patterns in the North Atlantic region (NAO and EA) and the Irish wave climate, contrasting the Atlantic and Irish Sea coasts.

In Fig. 14 the correlation between winter and spring yearly averages and NAO (retrieved from the Climate Prediction Center NOAA 2014b) for Hs, wave energy period (Tm) and wave peak direction (Pdir) are displayed. The areas with correlation significant at more than 95 % by Student's t test are hatched for clarity. As discussed by Bacon and Carter (1993), correlation coefficients greater than 0.5 signify a relatively strong connection between the wave climate and teleconnection patterns.

As can be seen in this figure, the Irish wave climate is highly influenced by the NAO pattern in winter. The significant wave height is directly correlated with NAO, with correlation coefficients exceeding 0.7 over most of the study area extent, with the exception of the nearshore eastern seaboard. These findings are consistent with similar studies (for example, Charles et al. 2012; Le Cozannet et al. 2010; Bertin et al. 2013; Dodet et al. 2010), which found positive phases of the NAO index to be associated with increased wave heights in the Northeast Atlantic in winter.

A significant positive correlation can be seen for the energy period on the west and northern coasts in winter, indicating an increase in energy period associated with positive NAO phases in these regions. For the peak wave direction, a statistically significant positive correlation is present on the southern and east coasts and in the Galway Bay on the west coast, corresponding to a northerly shift with increasing NAO indexes. In contrast, a negative correlation in direction (corresponding to a southerly shift) can be seen on the east coast. The positive correlation of wave heights and energy period with the NAO index persists on the west and northern coasts in spring. The summer and autumn wave climates are not impacted significantly by the NAO phase, with the exception of a negative correlation for significant wave heights in the southwest in summer which is consistent with the findings of Charles et al. (2012). This decrease in wave heights can be correlated with a strong high-pressure present over the southern part of Ireland, which is a feature of positive NAO phases in summer (as evidenced, for

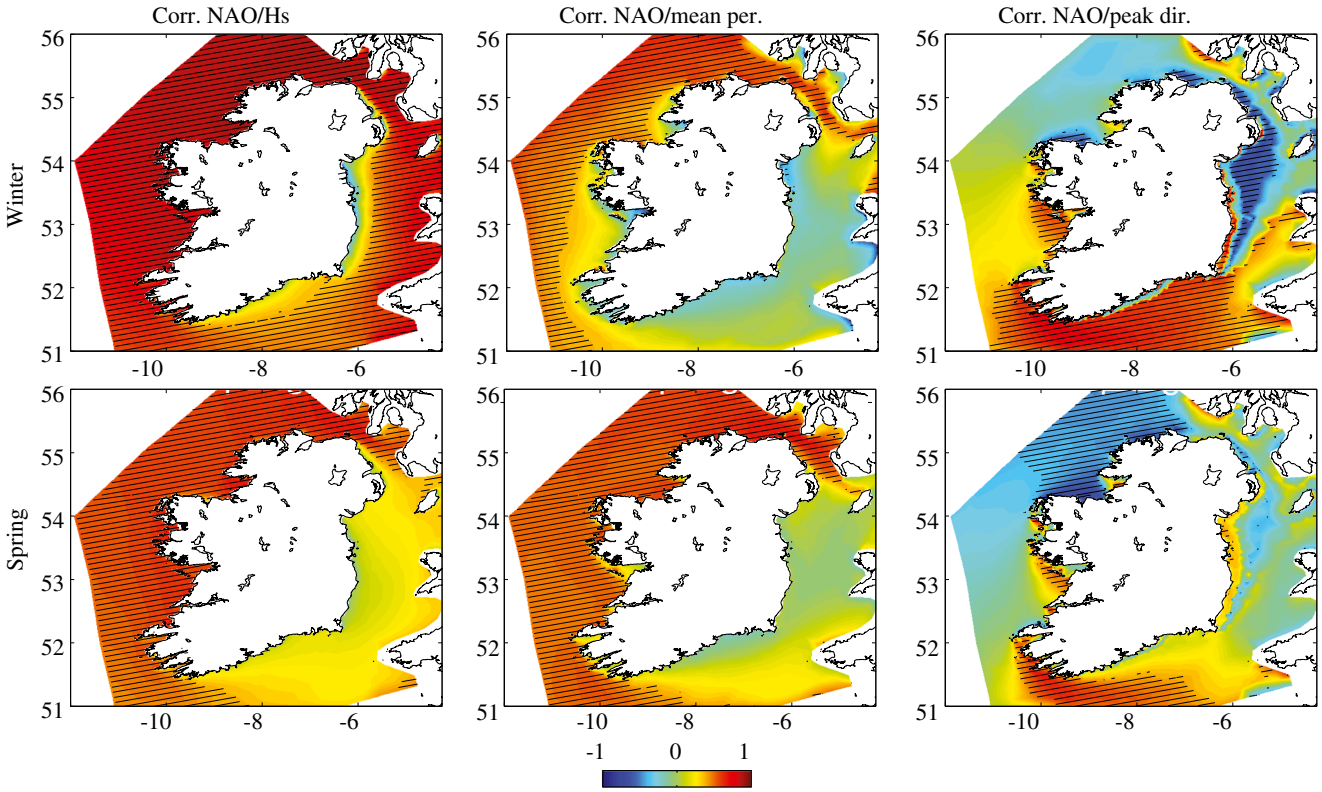

Fig. 14 Pearson correlation coefficient between NAO and seasonal averages (for winter and spring) of significant wave height, mean period and peak direction. Hatched: areas with correlation significant at higher than 95 % by t test

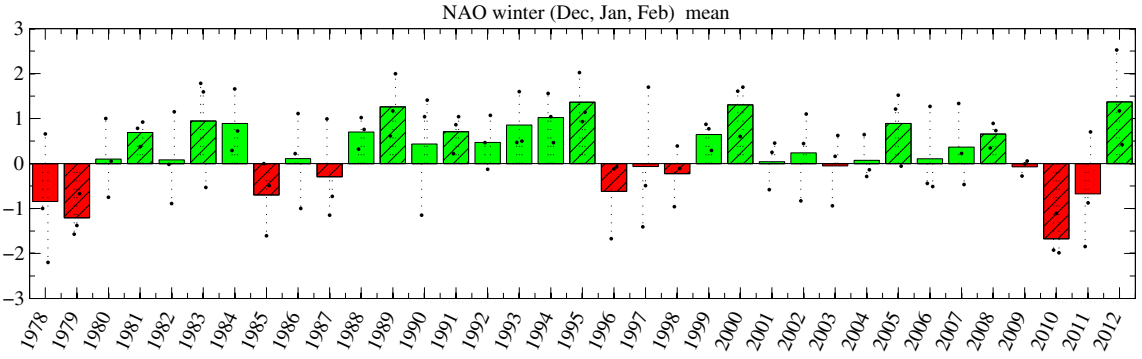

Fig. 15 Averaged winter (December, January, February) NAO index. Hatched: local minima/maxima. The monthly averaged NAO indexes for December, January and February of each year are depicted with *dashed lines*

example, by the maps of correlation between the standardised height anomalies and the NAO index, retrievable from the Climate Prediction Center NOAA 2014c).

Overall, the influence of the NAO on the Irish wave climate appears to be more significant than in other Northeast Atlantic regions (for example, as estimated by Charles et al. 2012 in the Bay of Biscay), in particular in winter and spring.

In the following, we take a closer look at the impact of the winter NAO phase (depicted in Fig. 15) on the wave climate

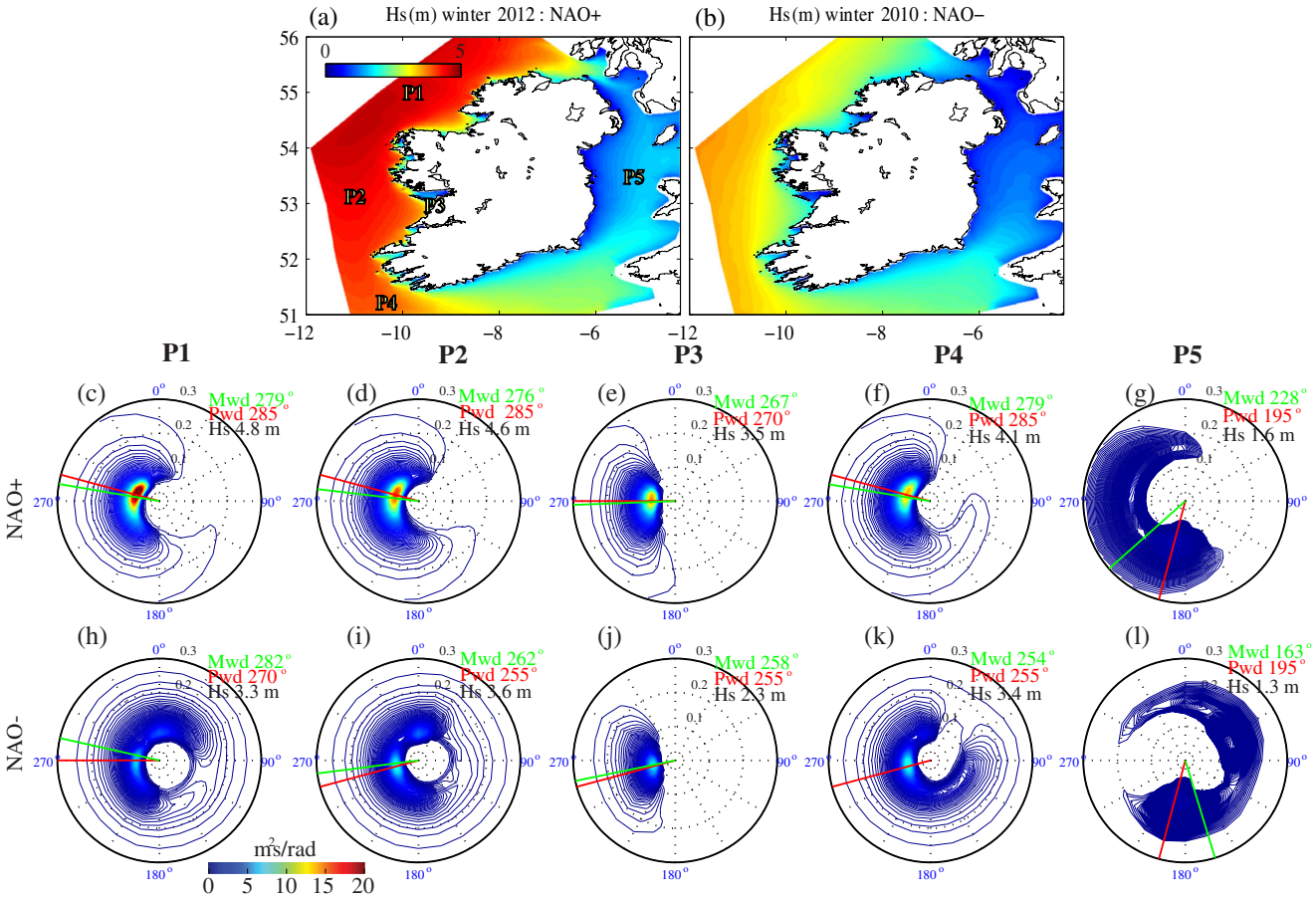

Fig. 16 Significant wave height for (**a**) winter 2012, corresponding to the maximum NAO winter index in the period of 1979–2012 (depicted in Fig. 15) and (**b**) winter 2010, corresponding to minimum NAO winter index during 1979–2012. **c**–**g** Averaged wave-variance density spectra (m^2s/rad) for winter 2012 at the locations depicted in panel (**a**). For each point, the average significant wave height, mean wave direction (Mwd) and peak wave direction (Pwd) are displayed. **h**–**l** Same as above, for winter 2010. (0° corresponds to waves coming from the north, and 90° from the east)

around Ireland. To this end, we evaluate the winter average significant wave height over the entire study area and the wave-variance density spectra at five points around the coast (depicted in panel a of Fig. 16) to contrast the following:

- the years corresponding to the maximum and minimum NAO phases that occurred during the 1979–2012 period (2012 NAO+ and 2010 NAO−, respectively)—results summarised in Fig. 16;
- the average over the years with local NAO maxima and local NAO minima—results summarised in Fig. 17.

The differences in wave heights between winter 2012 (NAO+) and 2010 (NAO−) (shown in panels a and b of Fig. 16) are staggering, in particular on the west coast, where decreases of more than 20 % can be seen. The contrast is only slightly diminished when wave heights averaged over years with extreme NAO positive phases and negative phases respectively are considered (see panels a and b of Fig. 17). Noteworthy also is the enhanced directional spread for the offshore points on the west coast (P1, P2 and P4) associated with the negative NAO indexes, in particular for the point P1, located in the northwest.

Furthermore, in the Irish Sea (point P5), the wave energy spectra exhibits a directional reversal between the NAO positive phase and negative phase, respectively (see panels g and l of Figs. 16 and 17, respectively). Indeed, negative phases of the NAO index generally give rise to a weakening of mid-latitude westerly winds with more occurrences of easterly winds in this region (Wilby et al. 1997; Castro-Díez et al. 2002). Interestingly, the point P3 located nearshore (at a depth of 60 m), exhibits smaller directional spread during negative NAO phases as opposed to positive NAO phases, presumably due to the sheltering effects of the Aran Islands which limit the fetch of the easterly winds. Finally, a northerly shift in both mean and peak direction associated with positive NAO phases can be seen at all points around the coast.

To conclude this section, we investigate the impact of the EA teleconnection pattern (retrieved from the Climate Prediction Center NOAA 2014b) on the Irish wave climate. The correlation maps between the wave climate seasonal averages (Hs, Tm and Pdir) and the EA for winter and autumn are displayed in Fig. 18, with areas of correlation, significant at more than 95 % by Student's t test, shown with hatching for clarity.

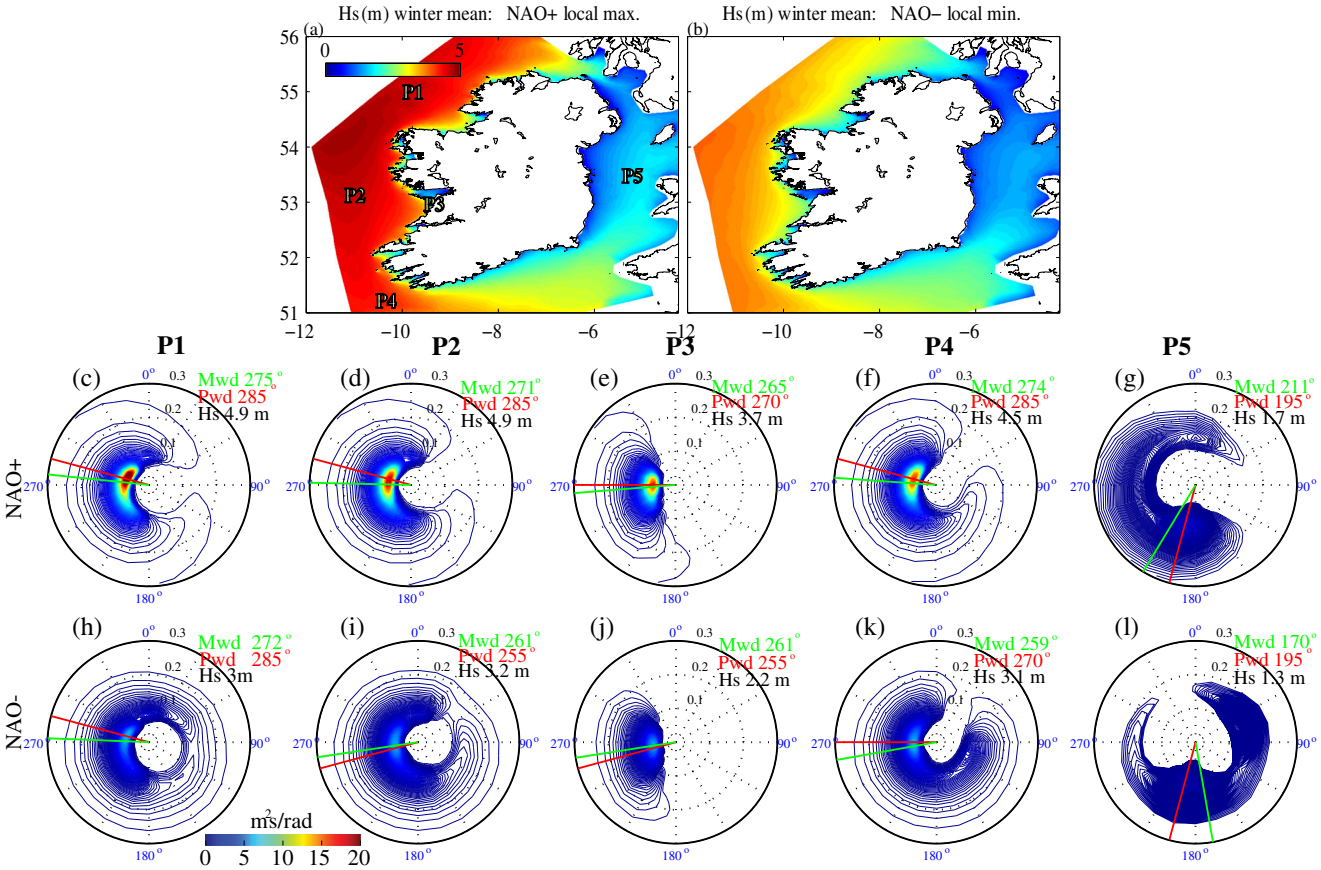

Fig. 17 Same as in Fig. 16, taking into consideration years with local maxima and minima respectively of the NAO winter index depicted in Fig. 15

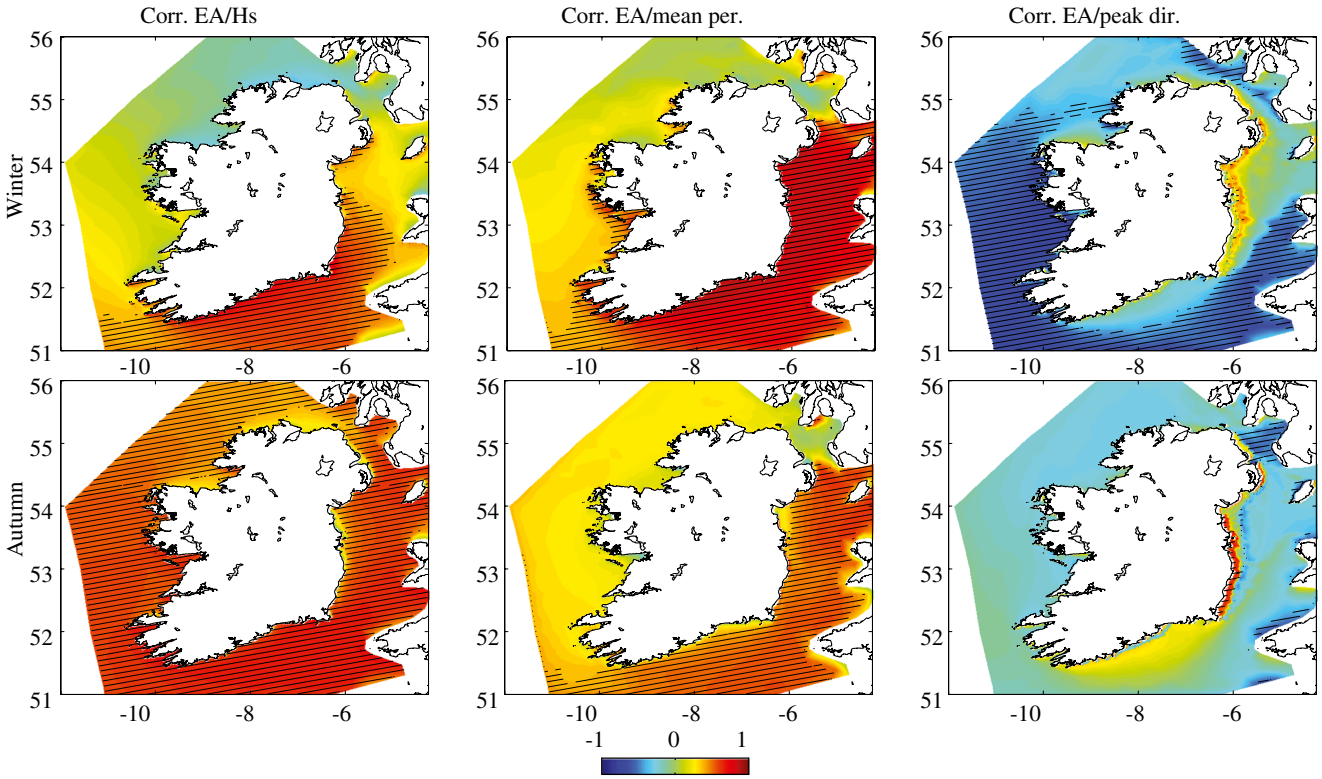

Fig. 18 Pearson correlation coefficient between EA and seasonal averages (for winter and autumn) of significant wave height, mean period and peak direction. Hatched: areas with correlation significant at higher than 95 % by *t* test

The most consistent connection with the EA index can be seen in autumn, in particular in the Irish Sea region and on the southern coast, where statistically significant positive correlations with the EA phase are present for both significant wave height and mean period. For this season, a positive correlation for the significant wave height can also be seen on the western coast.

The winter season presents significant correlations with the EA index for Hs and Tm on the southern coast. At the same time, the peak direction is inversely correlated with the EA phase, implying a southerly shift for increasing EA indexes.

Indeed, the positive phases of the EA are associated with a strong low-pressure located to the northwest of Ireland in autumn with a corresponding strong high in the north of Africa and over the Mediterranean (see, for instance, the maps of correlation between the standardised height anomalies and the EA, retrievable from the Climate Prediction Center NOAA 2014a). This situation leads to an intensification of southwesterly winds, and hence increased wave heights over the entire area around Ireland. Note also a slight southerly shift in peak wave direction (Fig. 18) and an increase in wave period in the Celtic and Irish Seas. For winter, the high is displaced southwards (southwest of Ireland). Hence, the area of increased wave heights is limited to the south of Ireland, in the Celtic Sea. The southerly shift in wave peak direction is amplified in this case, as well as the increase in wave mean periods. This could be attributable to an intensification of the wind, associated with an increase in the EA pattern strength in the winter season.

We note that significant positive correlations with Hs are also present in summer and spring (not shown here), in particular on the southern coast. However, the mean period and peak direction are not significantly affected by the EA phase in these seasons.

Overall, the EA appears to have less of an impact on the wave climate of Ireland in comparison with the NAO. The strongest correlation with the EA occurs in the autumn and persists throughout the seasons in the south and the south-east. This is in contrast to the NAO which dominates the wave climate on the west coast, particularly in winter and spring.

5 Summary and conclusions

A 34-year, high-resolution, nearshore wave hindcast was performed for Ireland, including both the Atlantic and the

Irish Sea coasts. The model was validated with observations from 17 wave buoys around Ireland and with altimeter data from the CERSAT database. The comparison between the observations and the model was found to be excellent. The lower quality of the model in the Irish Sea with respect to the western part of the model domain can be attributed to the different wave climate regimes in these regions (wind-sea versus swell dominated) in conjunction with the low spatial and temporal resolution of the forcing ERA-Interim wind fields. Indeed, comparing the ERA-Interim wind speed with altimeter measurements, a consistent low bias of around 5 % was found over the area of interest and an increased normalized root-mean-square error and bias variability in the Irish Sea basin.

Strong seasonal, interannual and spatial variability was found for the significant wave height and the wave energy flux. We have also identified a strong correlation between the NAO teleconnection pattern and wave heights, wave periods and peak direction in winter and, to a lesser extent, in spring. The NAO impacts predominantly the wave climate on the western coast. This is due to an intensification of the westerly winds at mid-latitudes across the North Atlantic basin associated with positive phases of the NAO index and, conversely, a weakening for negative phases. A large increase in mean wave heights and a northerly shift in peak wave direction were found for strong values of winter NAO positive phases. A significant correlation with the EA teleconnection pattern was identified in autumn. In contrast to the NAO, the EA teleconnection pattern influence can be seen in particular in the southern part of Ireland, due the positioning of the EA low-pressure centre to the west/southwest of Ireland.

Acknowledgements This study was funded by Science Foundation Ireland (SFI) under the research project "High-end computational modelling for wave energy systems" and by the Sustainable Energy Authority of Ireland (SEAI) through the Renewable Energy Research Development & Demonstration Programme. The ESB, Met Éireann, the Marine Institute and Shell provided the buoy data for validation. The INFOMAR bathymetric datasets were provided by the Geological Survey Ireland (GSI) and the Marine Institute. The VORF software for tidal datum conversions was obtained from the GSI. The UKHO bathymetry was provided by OceanWise Ltd. The altimeter-derived wave data was obtained from the Centre de Recherche et d'Exploitation Satellitaire (CERSAT), at Ifremer, Plouzané, France in the frame of the Globwave project, funded by the European Space Agency (ESA). The authors thank Dr. C. Sweeney and Prof. P. Lynch (UCD School of Mathematical Sciences) for very helpful discussions, Dr. F. Ardhuin (Ifremer) for his advice regarding the WAVEWATCH code, and M. Béchereau and P. Sweeney for their help with the construction of the DEM. Finally, the numerical simulations were performed on the Stokes cluster at the Irish Centre for High-end Computing (ICHEC) and at the Swiss National Computing Centre under the PRACE DECI 10 project "Nearshore wave climate analysis of the west coast of Ireland".

References

Appendini C, Camacho V (2012) Using GlobWave L2P data for wave hindcast assessments in the Gulf of Mexico. URL http://www.globwave.org/Tools/Case-Studies-Tutorials/Using-GlobWave-L2P-data-for-wave-hindcast-assessments-in-the-Gulf-of-Mexico/

Ardhuin F, Rogers E, Babanin A, Filipot JF, Magne R, Roland A, van der Westhuysen A, Queffeulou P, Lefevre JM, Aouf L, Collard F (2010) Semi-empirical dissipation source functions for wind-wave models: Part I, definition, calibration and validation. J Phys Oceanogr 40(9):1917–1941

Bacon S, Carter D (1993) A connection between mean wave height and atmospheric pressure gradient in the North Atlantic. Int J Climatol 13:423–436

Barnston A, Livezey E (1987) Classification, seasonality and persistence of low-frequency atmospheric circulation patterns. Mon Weather Rev 115:1083–1126

Berens P (2009) CircStat: a MATLAB toolbox for circular statistics. J Stat Softw 31(10)

Bertin X, Prouteau E, Letetrel C (2013) A significant incearse in wave-height in the North Atlantic Ocean over the 29th century. Glob Planet Chang 106:77–83

Boudière E, Maisondieu C, Ardhuin F, Accensi M, Pineau-Guillou L, Lespesqueue J (2013) A suitable metocean hindcast database for the design of marine energy converters. In: Proceedings of the 10th European wave and tidal energy conference series EWTEC, Aalborg

Cahill B, Lewis A (2011) Long term wave energy resource characterization of the Atlantic marine energy test site. In: Proceedings of the 9th European wave and tidal energy conference series EWTEC, Southampton

Calder B (2006) On the uncertainty of archive hydrographic data sets. IEEE J Ocean Eng 31(2):249–265

Castro-Díez Y, Pozo-Váquez D, Rodrigo F, Esteban-Parra M (2002) NAO and winter temperature variability in southern Europe. Geophys Res Lett 29(8):1–4

CERSAT (2013) Centre de Recherche et d'Exploitation Satellitaire (CERSAT). URL http://cersat.ifremer.fr/

Charles E, Idier D, Thiébot J, Le Cozannet G, Pedreros R, Ardhuin F, Planton S (2012) Present wave climate in the Bay if Biscay: spatiotemporal variability and trends from 1958 to 2001. J Clim 25(6):2020–2039

Climate Prediction Center NOAA (2014a) EA loading patterns. URL http://www.cpc.ncep.noaa.gov/data/teledoc/ea_map.shtml

Climate Prediction Center NOAA (2014b) NAO index. URL http://www.cpc.ncep.noaa.gov/data/teledoc/telecontents.shtml

Climate Prediction Center NOAA (2014c) NAO loading patterns. URL http://www.cpc.ncep.noaa.gov/data/teledoc/nao_map.shtml

COASTALT (2014) The COASTALT Project. URL http://www.coastalt.eu/

Curé M (2011) A fifteen year model based wave climatology of Belmullet, Ireland. Technical report. A report prepared on behalf of the Sustainable Energy Authority of Ireland (SEAI)

Dee DP, Uppala SM, Simmons AJ, Berrisford P, Poli P, Kobayashi S, Andrae U, Balmaseda MA, Balsamo G, Bauer P, Bechtold P, Beljaars ACM, van de Berg L, Bidlot J, Bormann N, Delsol C, Dragani R, Fuentes M, Geer AJ, Haimberger L, Healy SB, Hersbach H, Hólm EV, Isaksen L, Kållberg P, Köhler M, Matricardi M, McNally AP, Monge-Sanz BM, Morcrette JJ, Park BK, Peubey C, de Rosnay P, Tavolato C, Thépaut J-N, Vitart F (2011) The ERA-Interim reanalysis: configuration and performance of the data assimilation system. Q J of the R Meteorol Soc 137(656):533–597

Dias F, Gallagher S, Gleeson E, McGrath R, Tiron R, Whelan E (2013) Spatial and seasonal variability of the nearshore wave and

wind climate of Ireland: a high resolution hindcast for 2000-2012 with applications to the remewable energy sector. Technical report, Sustainable Energy Authority of Ireland

Dodet G, Bertin X, Taborda R (2010) Wave climate variability in the North-East Atlantic Ocean over the last six decades. Ocean Modell 31:120–131

Dorschel B, Wheeler A, Monteys X, Verbruggen K (2011) Atlas of the deep-water seabed. Springer, Ireland

EMODnet (2013) EMODnet. URL http://www.emodnet-hydrography.eu/content/content.asp?menu

ESB (2005) Accessible wave energy resource atlas of Ireland. Technical report, Report 4D404A-R2 for the Marine Institute and Sustainable Energy Ireland, ESB International

Folley M, Whittaker T (2009) Analysis of the nearshore wave energy resource. Renew Energy 34:1709–1715

Gallagher S, Tiron R, Dias F (2013) A detailed investigation of the nearshore wave climate and the nearshore wave energy resource on the west coast of Ireland. In: Proceedings of the ASME 2013 32nd International conference on ocean, offshore and arctic engineering OMAE, Nantes. American Society of Mechanical Engineers

GlobWave (2013) GlobWave project. URL http://www.globwave.org/

INFOMAR (2006) Integrated mapping for the sustainable development of Ireland's marine resource (INFOMAR): a successor to the Irish national seabed survey. Proposal & Strategy, Dublin

Janssen PAEM (2008) Progress in ocean wave forecasting. J Comput Phys 227:3572–3584

LANDSAT (2013) Global mosaic of Landsat7, courtesy nasa/jpl-caltech. URL http://ows.geogrid.org/basemap

Le Cozannet G, Lecacheux S, Delvallee E, Desramaut N, Oliveros C, Pedreros R (2010) Teleconnection pattern influence on sea-wave climate in the Bay of Biscay. J Clim 24:641–652

Liberti L, Carillo A, Sannino G (2013) Wave energy resource assessment in the Mediterranean, the Italian perspective. Renew Energy 50:938–949

MI (2013) Irish marine weather buoy network. URL http://www.marine.ie/home/publicationsdata/data/buoys/

Persson A (2011) User guide to ECMWF forecast products. Technical report, European Centre for medium-range weather forecasts (ECMWF), Reading

Poti M, Kinlan B, Menza C (2012) A biogeographic assessment of sea birds, deep sea corals and ocean habitats of the New York Bight: science to support offshore spatial planning. NOAA National Center for Coastal Ocean Science, chap. 2

Queffeulou P, Croizé-Fillon D (2013) Global altimeter SWH data set. Technical report, 10, Ifremer, Brest

Rascle N, Ardhuin F (2013) A global wave parameter database for geophysical applications. Part 2: model validation with improved source term parameterization. Ocean Modell 70:174–188

Roland A (2008) Development of WWM (Wind Wave Model) II: Spectral wave modelling on unstructured meshes. PhD thesis, Institute of Hydraulics and Wave Resource Engineering, Technical University Darmstadt, Germany

Rute Bento A, Marinho P, Campos R, Guedes Soares C (2011) Modelling wave energy resources in the Irish West Coast. In: Proceedings of the ASME 2011 30th international conference on ocean, offshore and arctic engineering, OMAE, Rotterdam. American Society of Mechanical Engineers

Taylor KE (2001) Summarizing multiple aspects of model performance in a single diagram. J Geophys Res 106(D7):7183–7192

Tiron R, Gallagher S, Dias F (2013) The influence of coastal morphology on the wave climate and wave energy resource of the West Irish Coast. In: Proceedings of the 10th European wave and tidal energy conference series EWTEC, Aalborg

Tolman H (2014) User manual and system documentation of Wavewatch III version 4.18. Technical report, 316, NOOA/NWS/NCEP/MMAB

Wang X, Swail V (2001) Changes of extreme wave heights in Northern Hemisphere oceans and related atmospheric circulation regimes. J Clim 14:2204–2221

Wang X, Swail V (2002) Trends of Atlantic wave extremes as simulated in a 40-year wave hindcast using kinematically reanalysed wind fields. J Clim 15:1020–1035

Wessel P, Smith W (1996) A global self-consistent, hierarchical, high-resolution shoreline database. J Geophys Res 101(B4):8741–8743

van der Westhuysen A (2012) Modeling nearshore wave processes. In: ECWMF Workshop on Ocean Waves, European Centre for medium-range weather forecasts, Reading

WestWave (2013) ESB WestWave project. URL http://www.westwave.ie/

Wilby R, O'Hare G, Barnsley N (1997) The North Atlantic oscillation and British isles climate variability, 1865–1996. Weather 52(9):266–276